TOXICOLOGICAL SCIENCES, 166(2), 2018, 451–464

doi: 10.1093/toxsci/kfy226
Advance Access Publication Date: September 10, 2018
Research Article

Evaluating Mode of Action of Acrolein Toxicity in an In Vitro Human Airway Tissue Model

Rui Xiong,* Qiangen Wu,† Levan Muskhelishvili,‡ Kelly Davis,‡ Jennifer M. Shemansky,* Matthew Bryant,† Hans Rosenfeldt,§ Sheila M. Healy,§ and Xuefei Cao*,1

*Division of Genetic and Molecular Toxicology; †Division of Biochemical Toxicology, National Center for Toxicological Research, US Food and Drug Administration, Jefferson, Arkansas 72079; ‡Toxicologic Pathology Associates, Jefferson, Arkansas 72079; and §Division of Nonclinical Science, Center for Tobacco Products, US Food and Drug Administration, Silver Spring, Maryland 20993

Disclaimer: This publication represents the views of the authors and does not represent FDA position or policy.
[1]To whom correspondence should be addressed at Division of Genetic and Molecular Toxicology, National Center for Toxicological Research, US Food and Drug Administration, 3900 NCTR Road, Jefferson, AR 72079. Fax: (870) 543-7393. E-mail: xuefei.cao@fda.hhs.gov.

ABSTRACT

Acrolein is a reactive unsaturated aldehyde and is found at high concentrations in both mainstream and side-stream tobacco smoke. Exposure to acrolein via cigarette smoking has been associated with acute lung injury, chronic obstructive pulmonary diseases (COPDs), and asthma. In this study, we developed an in vitro treatment strategy that resembles the inhalation exposure to acrolein experienced by smokers and systematically examined the adverse respiratory effects induced by the noncytotoxic doses of acrolein in a human airway epithelial tissue model. A single 10-min exposure to buffered saline containing acrolein significantly induced oxidative stress and inflammatory responses, with changes in protein oxidation and GSH depletion occurring immediately after the treatment whereas responses in inflammation requiring a manifestation time of at least 24 h. Repeated exposure to acrolein for 10 consecutive days resulted in structural and functional changes that recapitulate the pathological lesions of COPD, including alterations in the beating frequency and structures of ciliated cells, inhibition of mucin expression and secretion apparatus, and development of squamous differentiation. Although some of the early responses caused by acrolein exposure were reversible after a 10-day recovery, perturbations in the functions and structures of the air-liquid-interface (ALI) cultures, such as mucin production, cilia structures, and morphological changes, failed to fully recover over the observation period. Taken together, these findings are consistent with its mode of action that oxidative stress and inflammation have fundamental roles in acrolein-induced tissue remodeling. Furthermore, these data demonstrate the usefulness of analytical methods and testing strategy for recapitulating the key events in acrolein toxicity using an in vitro model.

Key words: acrolein; human air-liquid-interface (ALI) airway tissue model; oxidative stress; inflammatory response; goblet cell; squamous differentiation.

Acrolein, a highly reactive α,β-unsaturated aldehyde, is found ubiquitously as an environmental pollutant mainly as a result of the combustion of wood, diesel, and tobacco products. Human exposure to acrolein largely occurs via inhalation of mainstream and side-stream tobacco smoke (ATSDR, 2007). It is present in the gas phase of the mainstream cigarette smoke at levels between 3 and 220 μg per cigarette (Counts *et al.*, 2005; Dong *et al.*, 2000). Computational fluid dynamics modeling different breathing patterns (ie, nasal vs oral and steady-state vs transient) in several species reveals that deposition of inhaled acrolein is predominantly in the tracheobronchial regions of the lower respiratory tract and its uptake is predicted to be higher

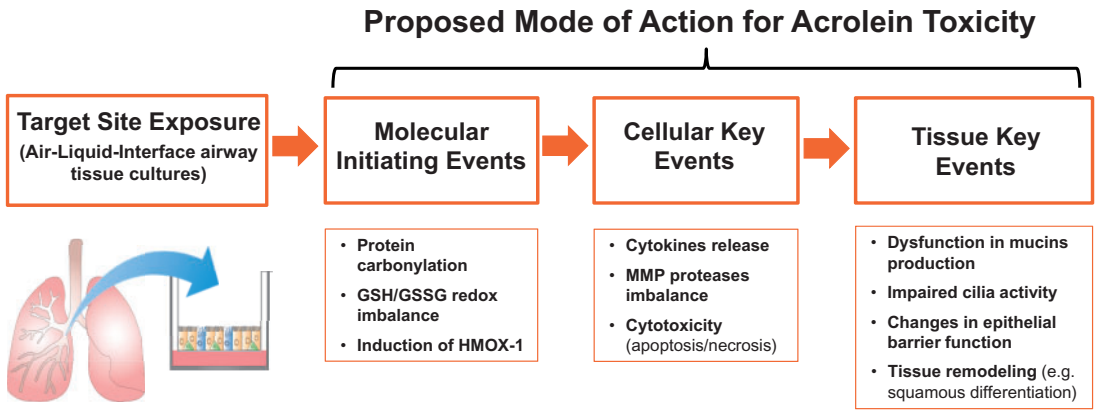

Figure 1. Schematic representation of the proposed MOA for acrolein toxicity in the ALI airway tissue cultures.

in humans than in rats or monkeys (Corley *et al.*, 2012, 2015). Due to its reactivity, exposure to acrolein is believed to be the most important risk factor for the development of a number of cigarette smoke-caused noncancer respiratory diseases, including chronic obstructive pulmonary disease (COPD) (Burcham, 2017; Moretto *et al.*, 2012).

There are very little toxicological data on human response to acrolein exposure, with most observations in humans focusing on nasal and eye irritation and its impact on respiratory rate (ATSDR, 2007). In animal models, inhalation exposure to acrolein at high levels (> 100 ppm) is found to induce oxidative stress, inflammatory responses, squamous metaplasia (SQM), bronchial lumen obstruction, bronchiolar epithelial cell hyperplasia, and necrosis in the lower respiratory tracts of the rats (reviewed in ATSDR, 2007; Beauchamp *et al.*, 1985; Catilina *et al.*, 1966). It is noteworthy that the inter-species difference in airway geometry, physiology, and breathing patterns greatly affects the regional tissue doses in the lung (Corley *et al.*, 2012). Thus, caution needs to be exercised when extrapolating toxicity between species. Nevertheless, there is a close resemblance between the acrolein-induced tissue responses observed in animal models and clinical symptoms observed in COPD patients. These observations, along with its high concentrations in mainstream and side-stream tobacco smoke, raise concerns over the long-term respiratory health effects of acrolein in both smokers and non-smokers.

Exposure and toxicity assessments traditionally have relied on data derived from animal models with specific genetic backgrounds. Even though there is moderate concordance between animal and human, extrapolation of animal data for human risk assessment involves the application of a number of uncertainty factors accounting for inter-species differences (Andersen and Krewski, 2010; Hartung and Daston, 2009). It would be useful to improve the scientific evidence supporting extrapolation from animal data to human data and consider alternative approaches that can potentially predict the disease-related tissue responses observed in humans.

Although mechanisms of acrolein toxicity, especially those at biochemical and molecular levels, have been extensively studied using monolayer cell models (Moghe *et al.*, 2015), acrolein-mediated airway tissue responses and remodeling have yet been evaluated due to the lack of suitable in vitro models. We have developed an in vitro test platform consisting of an in vitro air-liquid-interface (ALI) human airway tissue model bearing close resemblance to the structures and functions of human airway epithelium and a panel of toxicity endpoints relevant to tobacco smoke-associated respiratory diseases. By using such an in vitro system, we have successfully reproduced the key toxicity events that are induced by tobacco smoke or its constituents that occur in humans or lab animals (Cao *et al.*, 2015, 2017). These findings demonstrate the potential of such a test platform for generating disease-relevant tissue responses in vitro for evaluating health risks posed by inhaled toxicants under conditions reflecting real-life human exposures.

A mode of action (MOA) approach (U.S. EPA, 2003, 2005; Julien *et al.*, 2009) has been applied to define the key molecular events leading to the respiratory toxicity of acrolein (Yeager *et al.*, 2016). A similar, but more comprehensive adverse outcome pathway framework has recently been proposed for in vitro inhalation toxicity testing (Clippinger *et al.*, 2018). As revealed by the proposed MOA for acrolein, oxidative stress resulted from GSH conjugation and depletion leads to inflammation and subsequent cell death and tissue destruction and remodeling, which, in turn, causes enlarged lung airspaces and loss of lung elasticity. These key events occur consistently with the development of COPD. In this study, we aimed to reproduce the key in vivo toxicity events for acrolein using our in vitro test platform (Figure 1). A repeated treatment schedule (10 min/day for 10 days) was developed to understand the causal role of non-continuous acrolein exposure in smoke-associated respiratory diseases. The temporal responses of the various key events were delineated to elucidate the primary molecular initiating effects and adverse tissue responses that may lead to smoke-associated pulmonary diseases. Furthermore, the reversibility of acrolein-induced toxicity was examined to shed light on the effects of smoking cessation on these adverse tissue responses.

MATERIALS AND METHODS

Reagents and antibodies. Acrolein was purchased from Ultra Scientific (CAS No. 107-02-8; purity > 95%; North Kingstown, Rhode Island). Human placenta collagen type IV, mouse anti-β-actin antibody (AC-15), mouse anti-acetylated α-tubulin antibody (6-11B-1), SIGMA*FAST*™ Protease Inhibitor Cocktail, SIGMA*FAST*™ diaminobenzidine (DAB) Tablets, iodoacetamide (IAM), bovine serum albumin (BSA), and ExtrAvidin reagents were purchased from Sigma-Aldrich (St. Louis, Missouri). Glutathione ammonium salt-d5 (GSH-d5) and glutathione disulfide-$^{13}C_4^{15}N_2$ (GSSG-$^{13}C_4^{15}N_2$) were purchased from Toronto Research Chemicals Inc. (North York, Canada). Dulbecco's phosphate-buffered saline (DPBS, without calcium and

magnesium) was obtained from Cellgro (Manassas, Virginia). Rabbit anti-HMOX-1 and rabbit anti-cleaved caspase-3 (ASP175) antibodies were obtained from Cell Signaling Technology (Danvers, Massachusetts). Mouse anti-MUC5AC (45M1), mouse anti-involucrin (SY5) antibodies, TMB, and Permount Mounting Medium were purchased from Thermo Fisher Scientific (Waltham, Massachusetts). Mouse anti-MUC5B (19.4E) antibody was purchased from Abcam (Cambridge, Massachusetts). Mouse anti-GAPDH (G-9), mouse anti-CK6 (A-12), mouse anti-CK13 (AE8) antibodies, and dithiothreitol (DTT) were obtained from Santa Cruz Biotechnology (Dallas, Texas). M-PER Mammalian Protein Extraction Reagent, Pierce BCA Protein Assay, and Permount™ Mounting Medium were purchased from Fisher Scientific (Pittsburgh, Pennsylvania). Odyssey Blocking Buffer, IRDye 680RD goat anti-mouse IgG, and IRDye 680RD goat anti-rabbit IgG antibodies were obtained from LI-COR (Lincoln, Nebraska). HRP-conjugated goat anti-mouse IgG and goat anti-rabbit IgG secondary antibodies used for immunohistochemical staining were purchased from Vector Laboratories (Burlingame, California) and Sigma-Aldrich, respectively.

In vitro human air-liquid-interface (ALI) airway tissue model. Human ALI airway tissue models were established using the PneumaCult™-ALI Medium kit (STEMCELL Technologies, Canada) as described previously (Cao *et al.*, 2017). Briefly, cryopreserved normal human bronchial epithelial (NHBE) cells collected from lower respiratory bronchi tree with diameters equal to or larger than 2 mm (the Cystic Fibrosis Center Tissue Procurement and Cell Culture Core, University of North Carolina, Chapel Hill, North Carolina; Fulcher *et al.*, 2005) first were expanded in the PneumaCult™-Ex Medium (STEMCELL Technologies). When cells reached 90% confluence, cell pellets were collected and resuspended in PneumaCult™-Ex Medium to a concentration of 4.0×10^5 cells/ml. One hundred microliter cell suspension were added to each 24-well PET Transwell® culture inserts (Corning, Tewksbury, Massachusetts) precoated with human placenta collagen Type IV, with Expansion Medium being added to both the apical and basolateral compartments until cells reached 100% confluence. The PneumaCult™-ALI Maintenance Medium (STEMCELL Technologies) then was added to the basolateral compartments. And the medium was refreshed every other day for 4 weeks, by which time the cultures had become fully differentiated.

Acrolein treatment. Acrolein stock solutions were prepared by diluting neat acrolein in 10 ml LC-MS-grade water, pH 4.0, to concentrations between 140 and 160 mM. The stock solution was apportioned into 50-µl aliquots in sterile microcentrifuge tubes and stored at −80°C for up to 2 months. Treatment solutions were freshly made by diluting the stock solution in DPBS without calcium and magnesium (Cellgro, Manassas, Virginia) to concentrations between 125 and 1000 µM. After cultures were washed with DPBS, PneumaCult™-ALI Maintenance Media (400 µl) was added to the basal compartment and treatment solutions (35 µl) were added to the apical side of the ALI cultures and incubated for 10 min/day at 37°C, in the dark, for 10 consecutive days. At the end of each treatment, the treatment solution and the media in the basolateral compartment were aspirated and cultures were again washed with DPBS from the apical and basolateral sides. Cells were incubated in Maintenance Medium (400 µl) for 24 h until the next treatment. During the recovery period, the cultures were washed from the apical and basolateral sides and fresh Maintenance Medium added every other day for 10 days.

Cell viability assay. Cytotoxicity of acrolein was evaluated using the CellTiter 96® AQueous Non-Radioactive Cell Proliferation Assay (MTS assay; Promega, Madison, Wisconsin). The MTS working solution was prepared by diluting the stock solution in the PneumaCult™-ALI Maintenance Medium at a ratio of 1:5. Cell viability was assayed 24 h after the first treatment (T1) and 24 h after the last treatment (T10). Cultures were incubated in the MTS/PMS working solution (120 µl) from the apical side at 37°C for 1 h in the dark. Absorbance of the working solution (100 µl) was then measured using a BioTek Synergy H4 microplate reader (Winooski, Vermont). Cell viability is presented as the ratio of the absorbance produced by the treated groups to that in the control group.

Protein carbonyl ELISA. Protein oxidation was assessed by quantifying the intracellular levels of protein carbonyl using a Protein Carbonyl ELISA kit (CellBio Labs, San Diego, California). Protein lysate was prepared using the M-PER Mammalian Protein Extraction Reagent supplemented with SIGMA*FAST*™ protease inhibitor cocktail. Protein concentration was measured using the Pierce BCA assay. Cell lysate was diluted in DPBS to a final concentration of 10 µg/ml. Concurrent standards and samples were prepared per the manufacturer's recommendations. Briefly, the standards or samples (100 µl) were loaded into Nunc-Immuno™ MaxiSorp™ ELISA plates and incubated at 4°C overnight. Carbonyl groups were derivatized with DNPH (100 µl, 0.04 mg/ml) for 45 min at room temperature. Derivatized proteins were detected using an anti-DNP antibody (1:1000 dilutions in Blocking Solution). The optical density of protein carbonyl groups was determined at 450 nm with a BioTek Synergy H4 microplate reader. The fully reduced BSA standard was used as the background control. Protein carbonyl content was expressed as nanomole (nmol) protein carbonyl per mg protein.

Intracellular GSH and GSSG levels. The protocol for measuring the intracellular levels of GSH was modified from an HPLC-MS method described previously (Loughlin *et al.*, 2001). Briefly, the apical and basolateral sides of the cultures were washed with DPBS at each sampling time and ammonium bicarbonate buffer (pH 10.0) containing 10 mM IAM was added to the apical side of the cultures. The cells were then lysed by three rounds of freezing at −80°C and thawing at 37°C. The resulting cell lysate was collected by centrifugation at 10, 000 $\times g$ for 14 min at 4°C. Protein concentration was measured using the BCA assay and the samples were diluted in 10 mM IAM buffer (pH 10.0). Protein lysate was then deproteinized with acetonitrile containing 0.1% formic acid and 250 ng/ml internal standards, GSH-D5-IAM and GSSG-$13C_4$, $15N_2$. The samples were centrifuged at 10 000 $\times g$ for 5 min at room temperature and the supernatant (20 µl) was injected onto a Waters e2695 Alliance HPLC System coupled with a Waters ACQUITY QDa Mass Detector (Milford, Massachusetts). The GSH-IAM derivatives and GSSG were eluted on a Waters Atlantis T3 C18 column (4.6 × 150 mm, 5 µm). Elution was conducted at 40°C with a mobile phase of water (A) and acetonitrile (B), both containing 0.1% formic acid, at a flow rate of 0.5 ml/min. The column was flushed with 5% solvent B for 0.5 min, followed by a linear increase of solvent B from 5% to 50% over 4.5 min, returning to 5% solvent B over 0.5 min and maintaining at 5% solvent B for 6.5 min to re-equilibrate the column. The QDa mass spectrometer with an electrospray ion source operating in the positive ion mode (ESI+) and using selected ion recording (SIR) was used to detect the molecules of interest. The GSH-IAM, GSSG, GSH-d5-IAM, and GSSG-$13C_4$, $15N_2$ were monitored at *m/z* of 365.2, 307.2, 370.2, and 310.1,

respectively. GSH was quantified using calibration curves ranging from 0.625 to 40 μg/ml and for GSSG using 0.625 to 40 ng/ml in Waters Empower 3 software. The results were expressed as nmol analyte per mg protein.

Immunoblotting. Cells were lysed in the M-PER Mammalian Protein Extraction Reagent supplemented with SIGMAFAST™ Protease Inhibitor Cocktail and the protein concentrations measured using the BCA protein assay. Protein was denatured in a loading buffer containing DTT (50 mM) for 10 min at 90°C, loaded onto a NuPage® Novex® 4–12% Bis-Tris gradient gel (Life Technologies, Carlsbad, California). Proteins then were transferred onto a nitrocellulose membrane in an ice bucket at a constant voltage of 30 V for 1 h. Following a 1-h blocking in the Odyssey Blocking Buffer (LI-COR) at room temperature, proteins were visualized by incubating first with primary antibodies overnight at 4°C and then IRDye-conjugated secondary antibodies. Densities of the bands were quantified using the LI-COR Image Studio software.

Secretion of cytokines and MMPs. Secretion of select cytokines and MMPs into the basal medium was analyzed using a Bio-plex Pro Human Cytokine 27-plex assay kit and a Human MMP 9-plex assay kit, respectively (Bio-Rad, Hercules, CA). Basolateral media from treated ALI cultures and concurrent analyte standards were incubated with fluorescent magnetic beads with vigorous shaking at 850 ± 50 rpm for 1 h at room temperature. Excess reagents were removed by washing the plate three times with Wash Buffer. Proteins then were incubated with the Detection Antibodies, followed by three washes with Wash Buffer to remove the unbound antibodies. The protein-antibody conjugates were then labeled with streptavidin-PE. The beads were washed again with the Wash Buffer and resuspended in 125 μl Assay Buffer. Fluorescence of the beads was measured using a MAGPIX system (Luminex, Austin, Texas).

Mucin ELISA. MUC5AC and MUC5B were measured using an ELISA method. Apical washes from ALI cultures were collected into 200 μl DPBS. The disulfide bonds in the mucin were reduced by adding DTT to a final concentration of 0.025 mM. Cell debris was removed by centrifugation at 600 ×*g* for 10 min at 4°C. Fifty microliter apical wash were used for quantifying the secretion of MUC5AC and MUC5B. Whole cell proteins were extracted using the M-PER Mammalian Protein Extraction Reagent. Three μg and 5 μg of total proteins were used for quantifying the intracellular expression of MUC5AC and MUC5B, respectively. Mucin samples were added onto a NUNC-Immuno® MaxiSorp™ ELISA plate (Thermo Fisher Scientific) and allowed to dry in a humidified 37°C incubator overnight. Plates were blocked in 200 μl 5 mg/ml BSA solution with gentle shaking for 1 h at room temperature. Anti-MUC5AC or anti-MUC5B antibodies (50 μl), both diluted at 1:500 in DPBS containing 5 mg/ml BSA, 0.15% Triton™ X-100, and 0.1% Tween® 20, were added to each well and incubated for 2 h at room temperature. Following three washes with DPBS, HRP-conjugated goat anti-mouse IgG secondary antibodies (100 μL) were added and incubated for 1 h at room temperature. Color was developed using TMB substrate solutions (50 μl) and the reaction was stopped with 2 N HCl. Absorbance was measured immediately at 450 nm using a BioTek Synergy H4 microplate reader. An HRP-conjugated goat anti-mouse IgG secondary antibody was used in place of primary antibodies was used as the negative control.

Cilia beating frequency (CBF). CBF was measured using the Sisson-Ammons Video Analysis (SAVA) software and a high-speed camera as described previously (Sisson *et al.*, 2003). Measurements were made at 30°C on a heated stage. Four fields with at least 1000 motile points were randomly selected for each culture and an average was calculated. Three inserts were used for each treatment condition.

Histology and immunohistochemistry. Inserts were washed with DPBS and fixed in sufficient volume of 10% neutral buffered formalin for 48 h. Membranes were then excised from the plastic support, routinely processed, embedded in paraffin, sectioned to approx. About 4–5 μm thickness, mounted on positively charged glass slides, deparaffinized with xylene, rehydrated with ethanol solutions of decreasing concentrations, and stained with hematoxylin and eosin (H&E) using a Leica Autostainer (Buffalo Grove, Illinois).

For detection of goblet cells, tissue sections were oxidized in 0.5% periodic acid solution (PAS) for 5 min. The excess solution was removed by rinsing the sections in distilled water. The sections were then stained in Schiff's reagent for 15 min and was counter-stained with hematoxylin. The tissue sections were dehydrated first in ethanol solutions with increasing concentrations and then cleared in xylene. Goblet cell density was calculated by counting Periodic acid-Schiff (PAS) positive-stained cells over a 5-mm section.

For cleaved caspase-3 and CK13 immunohistochemistry, slides were placed in an antigen retrieval solution (0.01 M citrate buffer, pH 6.0) for 15 min in a microwave oven at 100°C at 800 W. For detection of involucrin, heat-induced epitope retrieval sections were incubated in 1 mg/ml trypsin for 5 min at 37°C. Tissue sections were then incubated in 3% hydrogen peroxide for 10 min to inactivate endogenous peroxidases. Nonspecific staining was blocked in 0.5% casein for 20 min. Antibodies against cleaved caspase-3, CK13, or involucrin (diluted 1:200, 1:100, and 1:100 in DPBS containing 1% BSA, respectively) were applied to the slides and incubated in a moisturized chamber for 1 h at room temperature. Following a 5-min wash in PBS, biotinylated goat anti-rabbit or anti-mouse secondary antibodies (diluted at 1:30 and 1:15, respectively) were applied to the tissue sections and incubated for 30 min at room temperature. After incubation with secondary antibodies, slides were washed and sections were incubated in ExtrAvidin peroxidase. Positively stained cells were visualized in DAB for 5 min at room temperature. Sections were counterstained with hematoxylin, dehydrated, and mounted with Permount Mounting Medium. Rabbit IgG were used in place of primary antibody to serve as the negative controls. The number of cleaved caspase-3-positive apoptotic bodies (ABs) were counted in tissue sections and expressed as number per mm.

Trans-epithelial electrical resistance (TEER). Changes in tissue permeability were evaluated by measuring the trans-epithelial electrical resistance (TEER) using an EVOM2 epithelial volt-ohmmeter (World Precision Instruments, Sarasota, Florida). Prior to each experiment, the EVOM was calibrated using a test electrode and the resistance was adjusted to 1000 Ω. Cell cultures were taken into the biological safety cabinet and equilibrated to room temperature. Two hundred μL DPBS were added to the apical compartment of the culture inserts. The background resistance was determined using an empty culture insert. Three measurements were made at positions 120 degrees apart for each culture and an average was calculated and used for data analysis.

Statistical analysis. All experiments were conducted at least three times and the data are presented as means ± standard error of

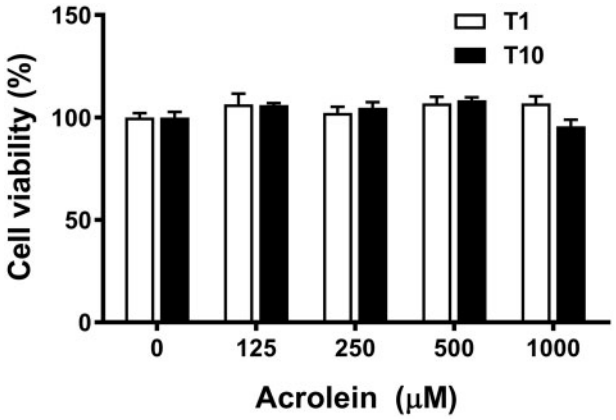

Figure 2. Cytotoxicity of acrolein in ALI airway models. ALI cultures were treated with acrolein from the apical side 10 min/day for 10 days. Cell viability was measured using the MTS assay 24 h after 1 (T1) and 10 (T10) treatments. Acrolein induced minimal cytotoxicity in ALI cultures after 10 repetitive exposures. Data ($n = 3$) are expressed as means ± SEM.

the mean (SEM). Statistical analysis was performed using the GraphPad Prism (La Jolla, California) and one-way analysis of variance (ANOVA) followed by Dunnett's multiple comparison tests.

RESULTS

Cytotoxicity-Induced by Acrolein

The cytotoxicity of acrolein was evaluated 24 h after 1 and 10 exposures using the MTS cell viability assay. Treatments of up to 1000 μM acrolein for 10 min per day for up to 10 days did not cause significant toxicity in the ALI cultures (Figure 2). Based on these observations, concentrations of up to 1000 μM were used for the subsequent toxicity studies.

Induction of Apoptosis by Acrolein

For evaluation of apoptosis, sections of ALI cultures were stained with a cleaved caspase-3 antibody 24 h after a 10-day treatment and at the end of a 10-day recovery. Although acrolein concentrations used for this study were noncytotoxic based on the MTS assay, high numbers of ABs were observed in areas with similar thickness as the DPBS-treated vehicle control at 1000 μM after 10 treatments (Figure 3A, T10). However, in thin areas (3–4 cell layers-thick) devoid of cilia and goblet cells and containing scattered angular squamoid epithelial cells, no ABs were found after a 10-day treatment (Figure 3A, T10). These thin areas were present only in the 1000 μM acrolein-treated cultures (immunostaining at other doses not shown). After a 10-day recovery, both tissue thickness and the number of ABs at the highest dose returned to the baseline level (Figure 3A, PT10). Quantification revealed a dose-dependent increase of ABs at concentrations up to 750 μM after 10 exposures (Figure 3B, T10). The thin areas in the 1000 μM acrolein-treated cultures were likely the reason why the average number of ABs in the 1000 μM acrolein-treated cultures were lower compared with the other treatment groups after a 10-day treatment. At the end of a 10-day recovery period, the number of ABs induced in all acrolein-treated groups returned to levels comparable to the controls (Figure 3B, PT10).

Protein Oxidation in Response to Acrolein Treatment

Intracellular levels of protein carbonyl were measured as one of the indicators of oxidative stress. Protein lysate was assayed

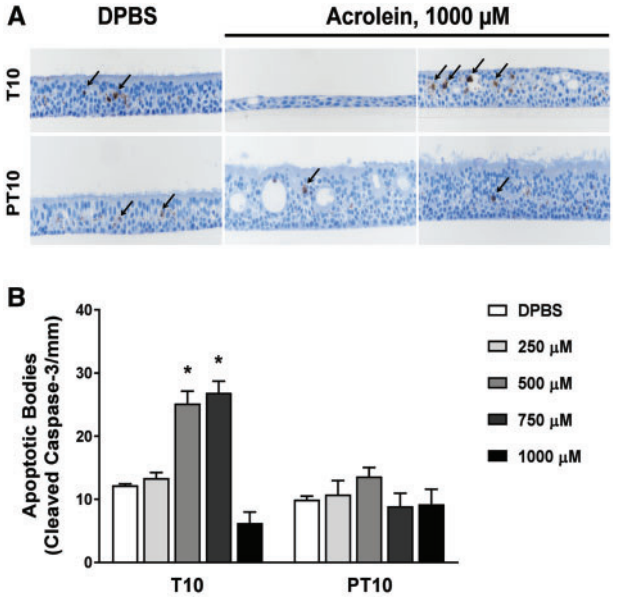

Figure 3. Reversible induction of apoptosis by acrolein exposure. Tissue sections of the ALI cultures were stained with a cleaved caspase-3 antibody 24 h after 10 treatments (T10) and 24 h after a 10-day recovery (PT10) using immunohistochemistry (A). Pictures were taken using 40× magnification. ABs (indicated by arrows) were counted and its density was calculated (B). Data ($n = 4$) are expressed as mean ± SEM. *$p < .05$ was considered statistically significant compared to the vehicle-treated controls.

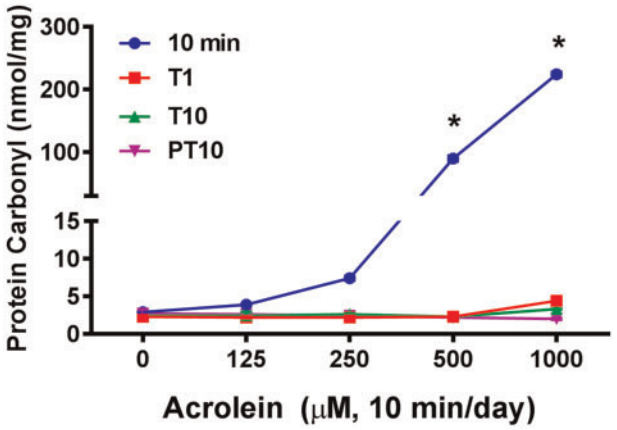

Figure 4. Protein oxidation in response to acrolein exposure. Formation of protein carbonyl by acrolein exposure were quantified immediately after a 10-min treatment (10 min), 24 h after 1 (T1) and 10 treatments (T10), and 24 h after a 10-day recovery (PT10). Data ($n = 3$) are presented as mean ± SEM. *$p < .05$ was considered statistically significant compared with the respective DPBS-treated vehicle control.

immediately after a 10-min treatment, 24 h after 1 (T1) and 10 treatments (T10), and 24 h after a 10-day recovery (PT10) (Figure 4). The levels of intracellular protein carbonyl were markedly increased immediately following a 10-min treatment. By the end of a 24-h recovery, protein oxidation was found to have returned to the baseline level.

Reversible Disruption of GSH/GSSG Redox Balance by Acrolein

Glutathione (GSH) is one of the major endogenous antioxidants synthesized by the cells. It plays a critical role in eliminating oxidative species induced by external insults, providing a

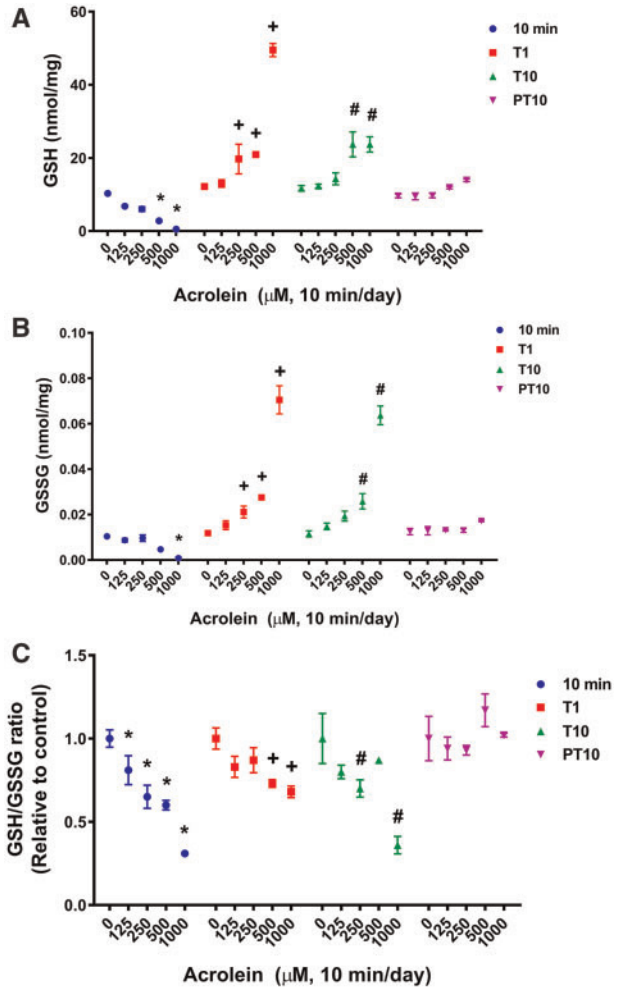

Figure 5. Disturbance of the GSH/GSSG redox balance by acrolein exposure. Intracellular levels of GSH (A) and GSSG (B) were quantified immediately after a 10-min treatment (10 min), 24 h after 1 (T1) and 10 treatments (T10), and 24 h after a 10-day recovery (PT10) using a LC-MS method. Note that changes in intracellular levels of GSH and GSSG at 10-min and T1 are linearly correlated with the administered concentrations of acrolein ($R^2 \geq 0.9$). Ratios of GSH/GSSG (C), an indicator of the intracellular redox balance, were calculated at the respective time points and normalized to their corresponding DPBS-treated vehicle controls. Data ($n = 3$) are expressed as mean ± SEM. *, +, #$p < .05$ was considered statistically significant compared to the respective DPBS-treated controls.

protective mechanism against oxidative stress (Lushchak, 2012). It has been reported that acrolein depletes intracellular low-molecular-weight thiols, such as GSH, without causing concomitant formation of oxidized GSH (GSSG) (Grafström *et al.*, 1988; Kehrer and Biswal, 2000). Consistent with the literature, we found a 10-min treatment with acrolein immediately decreased intracellular levels of GSH linearly in a dose-dependent manner (Figure 5A, 10 min). The highest acrolein dose also produced a slight decrease in GSSG content at this time point (Figure 5B, 10 min). However, when cultures were allowed to recover for 24 h, both GSH and GSSG levels were markedly increased in a dose-dependent manner (Figs. 5A and 5B, T1), regardless of the number of treatments (Figs. 5A and 5B, T10). Intracellular GSH and GSSG concentrations were restored to the baseline levels after a 10-day recovery (Figs. 5A and 5B, PT10). The ratios of GSH/GSSG exhibited dose-dependent decreases at all three time points throughout the treatment phase of the study (Figure 5C, 10 min, T1, and T10), suggesting a persistent

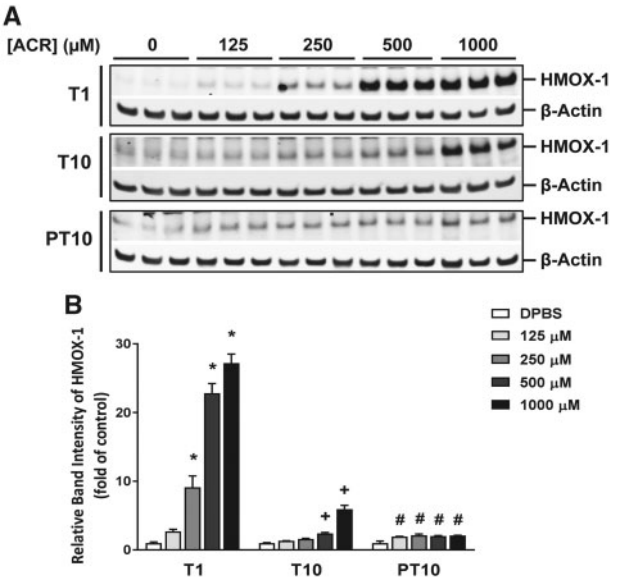

Figure 6. Time-dependent induction of HMOX-1 protein expression by acrolein exposure. Protein expression of HMOX-1 was evaluated 24 h after 1 (T1) and 10 treatments (T10) as well as 24 h after a 10-day recovery (PT10) by immunoblotting. β-Actin was used as the loading control. Representative immunoblots are presented in (A). Intensity of the HMOX-1 bands was quantified by densitometry and normalized to that of the loading control (B). Data ($n = 3$) are expressed as means ± SEM. *, +, #$p < .05$ was considered statistically significant compared with the respective DPBS-treated controls.

disruption of redox balance in the presence of acrolein. GSH/GSSG ratios were restored to baseline levels following a 10-day recovery (Figure 5C, PT10).

Induction of HMOX-1 by Acrolein

Induction of heme oxygenase-1 (HMOX-1) is an adaptive mechanism in response to oxidative stress induced by chemical exposures (Choi and Alam, 1996). The potential oxidative damage caused by acrolein was further evaluated by examining the expression of HMOX-1. Acrolein failed to induce HMOX-1 protein expression immediately after a 10-min treatment (data not shown). Twenty-four hours after the first treatment, HMOX-1 levels were increased in a dose-dependent manner, with 1000 μM acrolein causing a more than 27-fold increase in its expression (Figs. 6A and 6B, T1). The increase in HMOX-1 protein expression was attenuated after multiple treatments, although its levels in the acrolein-treated groups were still significantly greater than those of vehicle controls (Figs. 6A and 6B, T10). Induction of HMOX-1 by acrolein was diminished to nearly the control levels after a 10-day recovery period (Figs. 6A and 6B, PT10). This observation is in accord with the reversible effects of acrolein on protein oxidation and GSH/GSSG redox balance.

Secretion of Pro-Inflammatory Cytokines in Response to Acrolein Treatment

Exposure to acrolein causes the release of pro-inflammatory cytokines in human nasal and lung epithelial cells (Comer *et al.*, 2014; Sun *et al.*, 2014), which subsequently leads to chronic inflammation and structural changes in the lung (Barnes, 2009). Herein, we screened changes in the release of a panel of cytokines and chemokines using the Bio-plex Human Cytokine 27-plex multiplex assay. Release of 6 disease-related pro-inflammatory cytokines, ie, IL-1β, IL-6, IL-8, TNF-α, GM-CSF, and IFN-γ, was found to be significantly enhanced 24 h after the first

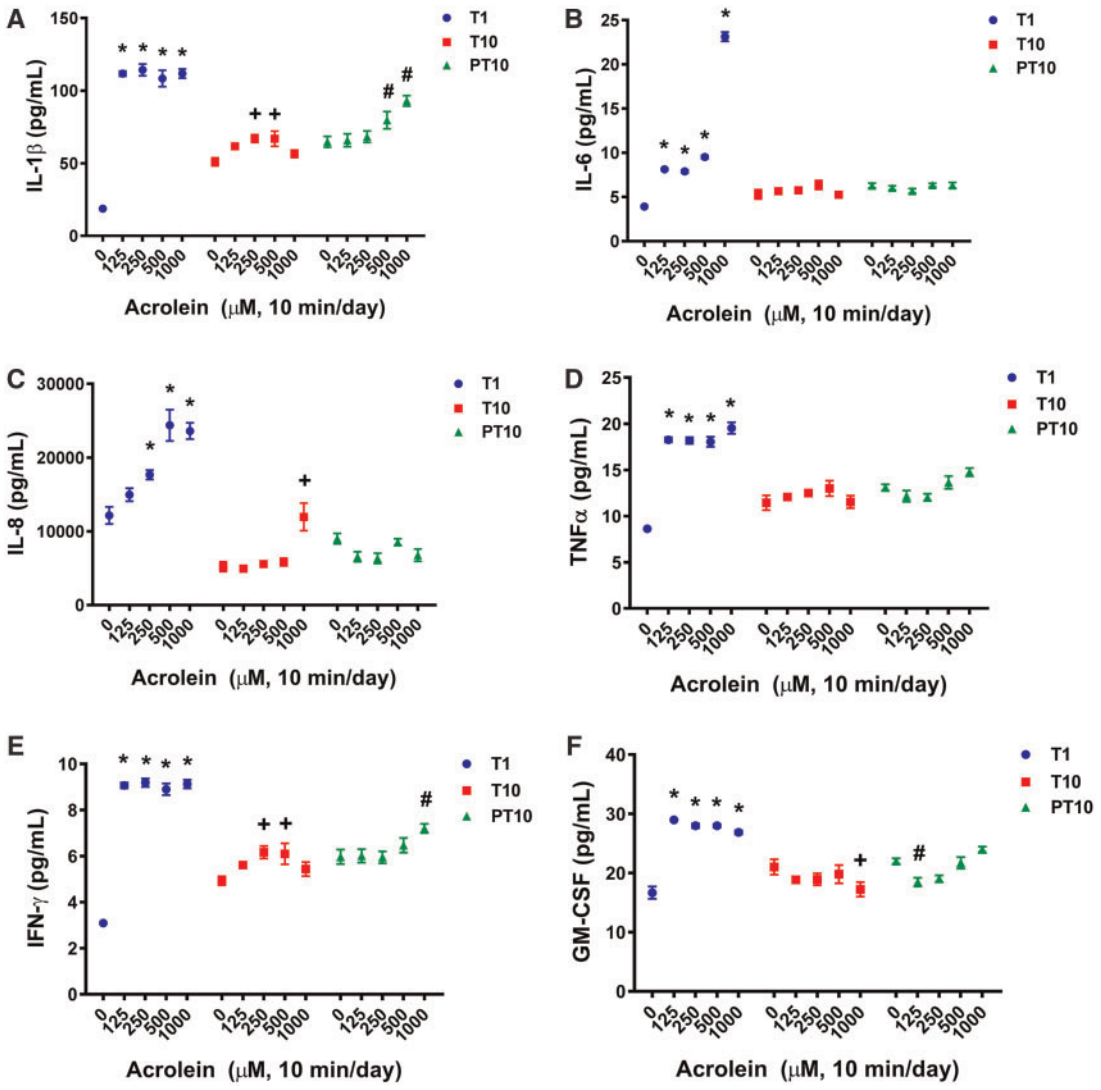

Figure 7. Secretions of pro-inflammatory cytokines induced by acrolein exposure. Secretions of select pro-inflammatory cytokines, ie, IL-1β (A), IL-6 (B), IL-8 (C), TNF-α (D), IFN-γ (E), and GM-CSF (F), in the basal medium were quantified using the Bio-Plex Pro Human 40-Plex 24 h after 1 (T1) and 10 treatments (T10) and 24 h after a 10-day recovery (PT10). Data ($n = 4$) are expressed as means ± SEM. *, +, #$p < .05$ was considered significant compared with their corresponding DPBS-treated vehicle controls.

10-min treatment (Figure 7, T1). Among these cytokines, secretion of the pro-inflammatory cytokines, IL-1β and IL-6, was increased approximately 6-fold by 1000 μM acrolein; release of the other four cytokines was stimulated approximately 2- to 3-fold by the same dose. It is pertinent to note that the secretion of IL-1β, TNF-α, IFN-γ, and GM-CSF was induced by the lowest concentration of acrolein and the induction was independent of the concentration. Changes in the secretion of IL-6 and IL-8, however, occurred in a dose-dependent manner. Repeated exposure to acrolein failed to further enhance the release of these cytokines (Figure 7, T10). In fact, the levels of all six cytokines in the basal medium were lower at T10 compared with T1. The concentrations of IL-6, TNF-α, and GM-CSF returned to baseline levels after 10 treatments. Secretion of IL-8 remained elevated only at the highest dose, suggesting its possible role in acrolein-mediated tissue remodeling (eg, squamous differentiation). After a 10-day recovery, the secretion of all six cytokines, except IL-1β, returned to near baseline levels (Figure 7, PT10).

Disturbance of MMP Homeostasis by Acrolein

Acrolein induces MMP proteins in transgenic rodent models and human cell lines in vitro (Deshmukh *et al.*, 2008; Lemaître *et al.*, 2011; O'Toole *et al.*, 2009). Using our treatment schedule, we found that acrolein induced the release of multiple MMPs, including MMP-7, MMP-10, MMP-12, and MMP-13 (Figure 8). Twenty-four hours after the first exposure, secretion of MMP-7 and MMP-10 was altered in a dose-dependent manner, with secretion of MMP-7 being increased and MMP-10 being decreased (Figs. 8A and 8B, T1). Changes in MMP-13 secretion appeared to be bi-phasic, with lower doses increasing and the highest dose decreasing its release after a single exposure (Figure 8D, T1). After 10 repeat exposures, acrolein modulated the secretions of MMP-7 and MMP-10 in a bi-phasic manner, similar to that observed with MMP-13 after a single exposure (Figures 8A and 8B). Secretion of MMP-13 was induced at this time point (Figure 8D). The highest concentration of 1000 μM significantly decreased the secretion of MMP-12 after 10 treatments (Figure 8C, T10). At the end of the 10-day recovery period, the

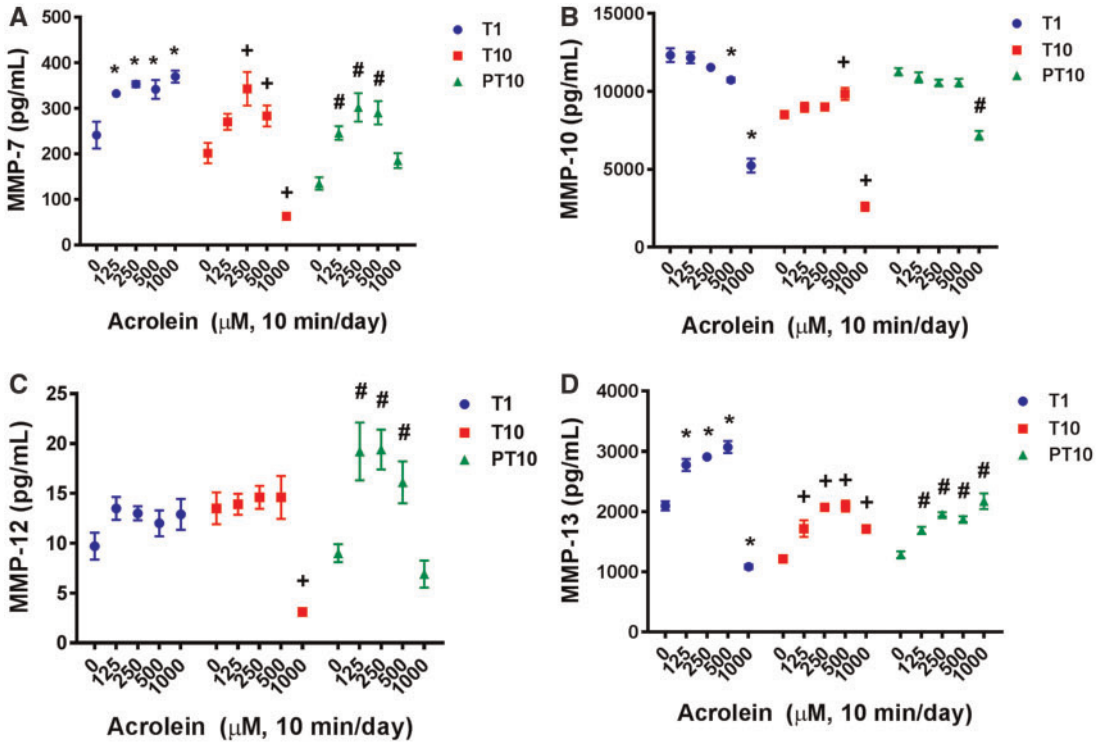

Figure 8. Disturbance of MMP homeostasis by acrolein exposure. Secretions of select MMP proteins, ie, MMP-7 (A), MMP-10 (B), MMP-12 (C), and MMP-13 (D), in the basal medium were quantified using the Bio-Plex Human MMP 9-Plex 24 h after 1 (T1) and 10 treatments (T10) and 24 h after a 10-day recovery (PT10). Data ($n = 4$) are expressed as means ± SEM. *, +, #$p < .05$ was considered statistically significant compared with their respective DPBS-treated controls.

secretion of MMP-7 and MMP-12 was restored to baseline levels at the highest dose, but remained increased at the lower doses (Figs. 8A and 8C, PT10). Acrolein-induced release of MMP-10 was attenuated after the recovery phase (Figure 8B, PT10), whereas the level of MMP-13 remained relatively unchanged at PT10 compared with that at T10 (Figure 8D, PT10).

Regulation of Mucin by Acrolein

Regulated expression and secretion of MUC5AC and MUC5B, the major mucins predominantly expressed in airway epithelium, are essential for maintaining respiratory health (Almolki *et al.*, 2008; Hauber *et al.*, 2006). Evaluation of the effects of acrolein on their intra- and extra-cellular levels revealed that MUC5AC (Figure 9), but not MUC5B (data not shown), was modulated by acrolein exposure in the ALI cultures. Secretion of MUC5AC was stimulated by 1000 μM acrolein 24 h after the first treatment (Figure 9A, T1). After 10 repetitive exposures, secretion of MUC5AC in the group treated with the highest concentration of acrolein was reduced compared with that in the vehicle-treated control (Figure 9A, T10). This reduction was also observed after the recovery period (Figure 9A, PT10).

Protein expression of MUC5AC, on the other hand, was suppressed by acrolein exposure 24 h after the first 10-min treatment, yet the inhibition did not reach statistical significance (Figure 9B, T1) until 10 repeated exposures (Figure 9B, T10). The inhibition of MUC5AC expression was reversed only at the lower doses (ie, doses up to 500 μM) after a 10-day recovery (Figure 9B, PT10), suggesting irreversible morphological changes caused by acrolein exposure at the highest dose.

Staining for goblet cells in cultures treated for up to 10 days revealed that 1000 μM acrolein altered the morphology of the airway epithelial tissue models (Figure 9C, T10). Treatment effect was manifested as decreased epithelial thickness (3–4 cell layers thick), scattered angular squamoid epithelial cells, and loss of ciliated and goblet cells (Figure 9C, T10, middle panel). The goblet cells in sections with normal thickness appeared to be disrupted (Figure 9C, T10, right panel). Quantification of goblet cell density confirmed that the highest concentration of acrolein decreased the number of goblet cells by approx. 8-fold after 10 repetitive treatments (Figure 9D, T10). Tissue structures were partially restored 10 days after cessation of the treatment and the thickness of the tissue was greater than that of the PBS-treated vehicle control (Figure 9C, PT10). However, the goblet cell density failed to completely return to the baseline level (Figure 9D, PT10), which is consistent with the persistent inhibition of MUC5AC secretion and protein expression by acrolein treatment observed at the end of a 10-day recovery (Figure 9C, PT10).

Functional and Possible Structural Changes of Ciliated Cells by Acrolein

Intact, functioning ciliated cells are an indispensable component of the mucociliary clearance mechanism (Tilley *et al.*, 2015). The highest concentration of acrolein significantly increased the cilia beating frequencies (CBF) 24 h after the first treatment (Figure 10A, T1). Repetitive exposures, however, resulted in approximately 30% decrease in CBF (Figure 10A, T10), which was then completely restored to the baseline level after a 10-day recovery (Figure 10A, PT10). Because suppression of CBF suggested structural changes to the ciliated cells, we measured the expression of a protein marker for cilia structure, acetylated α-tubulin, during the treatment and recovery phases of experiment. Protein expression of acetylated α-tubulin was not changed 24 h after the first treatment, suggesting that possible structural changes did not occur at this time point

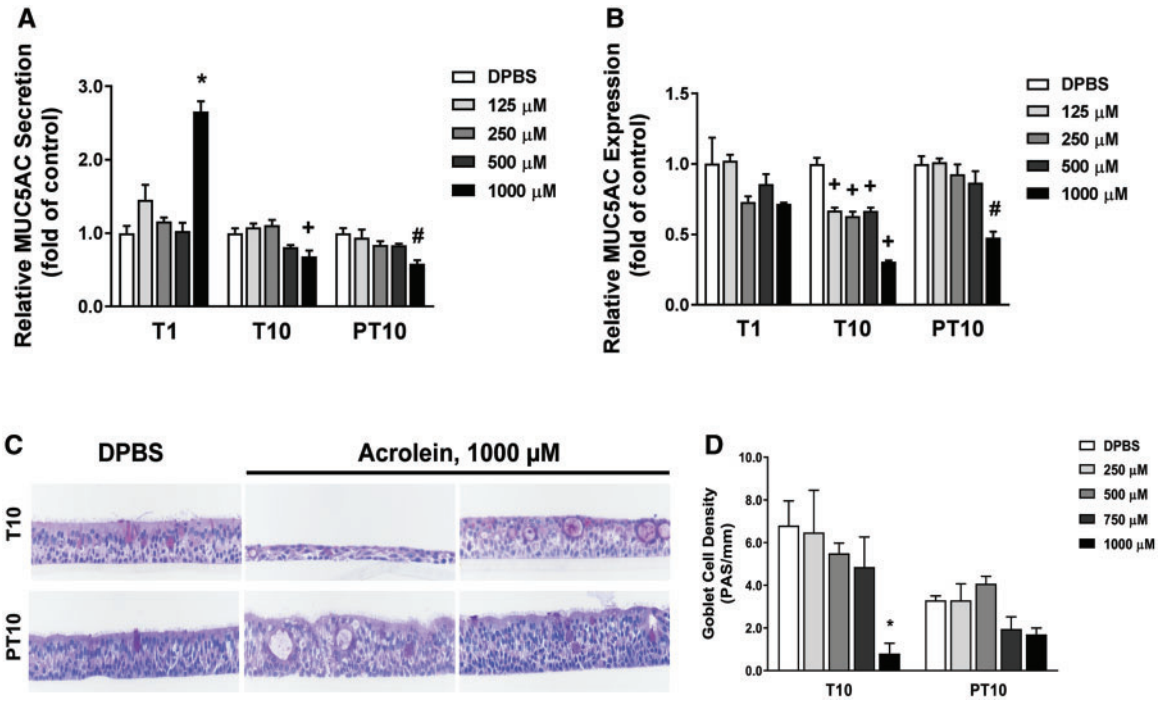

Figure 9. Effects of acrolein on mucin homeostasis. Secretion (A) and expression (B) of MUC5AC were evaluated 24 h after 1 (T1) and 10 treatments (T10) as well as 24 h after a 10-day recovery (PT10). Goblet cells were stained using PAS 24 h after 10 treatments (T10) as well as 24 h after a 10-day recovery (PT10) (C). Goblet cell density was calculated as the ratio of the cell number to the length of the tissue section (D). Data ($n = 6$ for MUC5AC secretion, $n = 3$ for MUC5AC expression, and $n = 4$ for PAS staining) are expressed as means ± SEM. *, +, #$p < .05$ was considered statistically significant compared with their respective DPBS-treated controls.

(Figures 10B and 10C, T1). When the ALI cultures were repeatedly exposed to acrolein for 10 days, the expression of acetylated α-tubulin was decreased (Figures 10B and 10C, T10); a 10-day recovery period failed to restore its expression (Figures 10B and 10C, PT10).

Squamous Differentiation Induced by Acrolein

SQM is a common morphological change observed in habitual smokers as well as in laboratory animals exposed to acrolein (Dorman *et al.*, 2008; Rigden *et al.*, 2016). It is initiated as a self-protective mechanism to remove potential pathological lesions caused by chemical exposures (Puchelle *et al.*, 2006). We examined the changes in the staining pattern as well as the expression of select protein markers for squamous differentiation, including involucrin, CK13, and CK6 (Araya *et al.*, 2007), in ALI cultures repetitively exposed to 10 treatments with acrolein (Figure 11A, T10). Exposure to acrolein at 1000 μM caused heterogeneous squamous differentiation across the tissue sections. Areas of thin and scattered epithelial cells were observed in the ALI cultures. Cells within these affected areas had a squamoid cell appearance consisting of angular cell borders and enlarged cytoplasm. Other areas within the same cultures appeared to be normal with respect to both cell structures and thickness, although intraepithelial cysts were consistently found in these areas (Figure 11A, H&E at T10). Staining of both involucrin and CK13 was concentrated in the cytoplasm of the affected epithelial cells (Figure 11A, involucrin and CK13 at T10). CK13 also was found to be increased in areas with normal thickness, suggesting it may be a biomarker for the early stage of squamous differentiation. Immunoblotting confirmed the significant up-regulation of CK13 and involucrin as well as a slight increase in the expression of an additional squamous differentiation biomarker, CK6 (Figs. 11B and 11C, T10). Preliminary pathology staining on tissues treated 10 min/day for 4 days revealed no aberrant tissue remodeling; the aforementioned morphological changes occurred only after a 10-day treatment. After a 10-day recovery, the thickness of the treated cultures was not only restored, but became thicker than that of the DPBS-treated vehicle control (Figure 11A, PT10). Intraepithelial cysts as well as the staining of CK13 persisted in certain areas of the acrolein cultures after a 10-day recovery period. However, immunoblotting revealed sustained up-regulation of all three squamous differentiation biomarkers at the end of a 10-day recovery (Figures 11B and 11C, PT10), indicating that squamous differentiation induced by acrolein may have not been fully reversed under these experimental conditions. In accord with these changes in the structure of ALI cultures, we also found that tissue integrity, as measured by TEER, was moderately altered by the acrolein treatment (Figure 11D). Twenty-four hours after the first treatment, tissue integrity of the cultures was decreased approximately 50% by 1000 μM acrolein (Figure 11D, T1). Repetitive exposures, however, significantly increased the trans-epithelial resistance at the highest dose (Figure 11D, T10) and the increase was sustained until the end of a 10-day recovery period (Figure 11D, PT10).

DISCUSSION

Acrolein is a toxic respiratory irritant present in environmental pollutants and tobacco smoke. Concentrations of acrolein usually range from 0.02 to 12 ppb in environmental pollutants, but exceed 50 ppm per cigarette in mainstream smoke and are found to be several-fold higher in side-stream smoke (Brunnemann *et al.*, 1990; National Research Council (US) Committee on Passive Smoking, 1986). Consequently, compared with the general population, both habitual smokers and

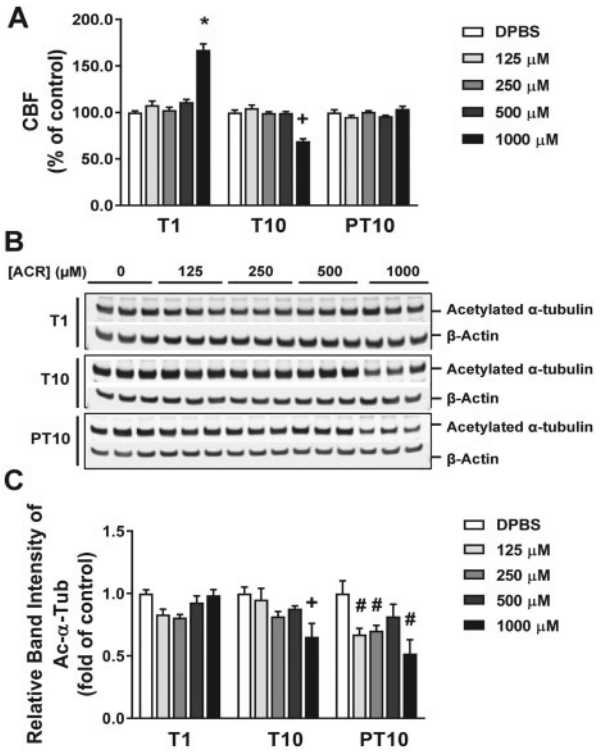

Figure 10. Impairment of cilia functions by acrolein exposure. CBF was measured 24 h after 1 (T1) and 10 treatments (T10) as well as 24 h after a 10-day recovery (PT10) (A). Protein expression of acetylated α-tubulin was evaluated at the same time points by immunoblotting (B). Densitometry was conducted to quantify the intensity of the bands and the expression of acetylated α-tubulin is expressed as relative fold change to the β-actin loading control (C). Data ($n = 3$) was expressed as means ± SEM. *, +, #$p < .05$ was considered statistically significant compared with their respective DPBS-treated controls.

nonsmokers passively inhaling second-hand smoke are exposed to elevated levels of acrolein (ATSDR, 2007). Considering the potential for adverse health effects from chronic exposure to acrolein through smoking, developing testing strategies for generating toxicity data to inform human health risk assessments of tobacco products is useful. In the present study, we evaluated the tobacco smoke-associated toxicity of acrolein using a well-differentiated human airway epithelial tissue model and a novel treatment protocol that represents bronchial exposure to acrolein in active smoking. By using such a treatment regimen, progression of changes in tissue responses induced by acrolein can be monitored.

Acrolein rapidly forms adducts with intracellular macromolecules upon contact via Michael addition (LoPachin *et al.*, 2009), resulting in protein carbonylation. Due to its extremely high reactivity, measuring free form of acrolein in tissues is difficult. Therefore, quantitation of acrolein conjugates, such as carbonylated proteins, has been used as a potential surrogate indicator for estimating the levels of acrolein exposure (Burcham, 2017). Immunoblotting has been widely used for measuring intracellular protein carbonyls (Avezov *et al.*, 2014; Burcham, 2004). However, immunoblotting data generated using such a method are semiquantitative and often lack of reproducibility (Augustyniak *et al.*, 2015). Herein, we applied a sensitive ELISA technique that detects intracellular protein carbonyls of both low and high abundance. Our data demonstrated that the induction of protein carbonyls is linearly correlated with the administered concentrations of acrolein immediately after a 10-min exposure ($R^2 = 0.955$). Repetitive exposures, however, did not result in the accumulation of protein carbonyls. Instead, the concentrations of carbonyls returned to baseline level 24 h after each treatment, possibly due to two potential mechanisms. First, the carbonylated proteins may have been efficiently degraded via either a proteasome-mediated pathway or autophagy (Cuervo *et al.*, 2005; Davies, 2001) Second, the labile acrolein-cysteine conjugates, which are the predominant forms of acrolein-protein adducts, readily cross-react with other proteins (Burcham *et al.*, 2007; Cai *et al.*, 2009). If either or both pathways are involved, protein carbonyl accumulation will not be detected under these experimental conditions. Nevertheless, our observations suggest that protein carbonyl may be used as a non-specific exposure marker for acute, but not sub-chronic or chronic acrolein exposures.

Acrolein preferentially reacts with free thiols, such as GSH (LoPachin *et al.*, 2009). Consistent with previous findings, we demonstrate that acute (ie, 10 min) exposure to acrolein rapidly depletes intracellular GSH with minimal induction of GSSG (Grafström *et al.*, 1988; Kehrer and Biswal, 2000). Significant concentration-dependent increases in GSH and GSSG levels were detected 24 h after each treatment, suggesting that the GSH synthesis pathway may have been triggered as an adaptive response to acrolein exposure (Gao *et al.*, 2015). These findings suggest that the primary action of acrolein is to deplete GSH, which, in turn, may interfere with redox homeostasis and subsequently leads to sustained oxidative stress. Changes in the HMOX-1 protein expression in response to acrolein exposure are also temporally correlated with changes in the GSH/GSSG ratios, indicating that acrolein exposure leads to oxidative stress in the ALI models. Although acrolein-mediated oxidative stress is partially reversible, oxidative damage resulting from early exposure may contribute to the functional abnormalities observed with repeated exposures in the ALI cultures. These results suggest that the intracellular levels of GSH and GSSG as well as their ratios may reflect acrolein-mediated adverse effects and, therefore, may be used as a biomarker for acrolein exposure and toxicity.

Mucins are polymeric glycoproteins that function as cellular defense molecules against respiratory toxicants (Fahy and Dickey, 2010). Dysfunctions in mucin production, secretion, and clearance have been recognized as a key etiological factor for cigarette smoking-associated respiratory diseases, such as COPD (Almolki *et al.*, 2008). The effects of acrolein on mucins, particularly MUC5AC, have been studied extensively in vitro and in vivo. Most of these studies report that exposures to low levels of acrolein (3 ppm) induce the expression of MUC5AC (Deshmukh *et al.*, 2008; Borchers *et al.*, 1998; Rahimi, 1999). In our study, however, we found that MUC5AC secretion increased transiently after the first treatment, while repeated exposure inhibited its expression and secretion, both of which may be caused by the loss of goblet cells observed in the acrolein-treated cultures.

In normal airway epithelium, the efficiency of mucociliary clearance is maintained by the coordinated activities of secretory cells and ciliated cells (Knowles and Boucher, 2002). Acrolein is a potent ciliastatic toxicant (Beauchamp *et al.*, 1985) and has been associated with cigarette smoke-induced cilia toxicity (Aufderheide *et al.*, 2015; Walker and Kiefer, 1966). However, we are not aware of any detailed reports on the effects of repeated acrolein exposure on cilia functions in ALI airway tissue models. Herein, we demonstrated that CBF was temporarily accelerated, which may be seen as a stress response to remove the toxicants, 24 h after the first acrolein exposure.

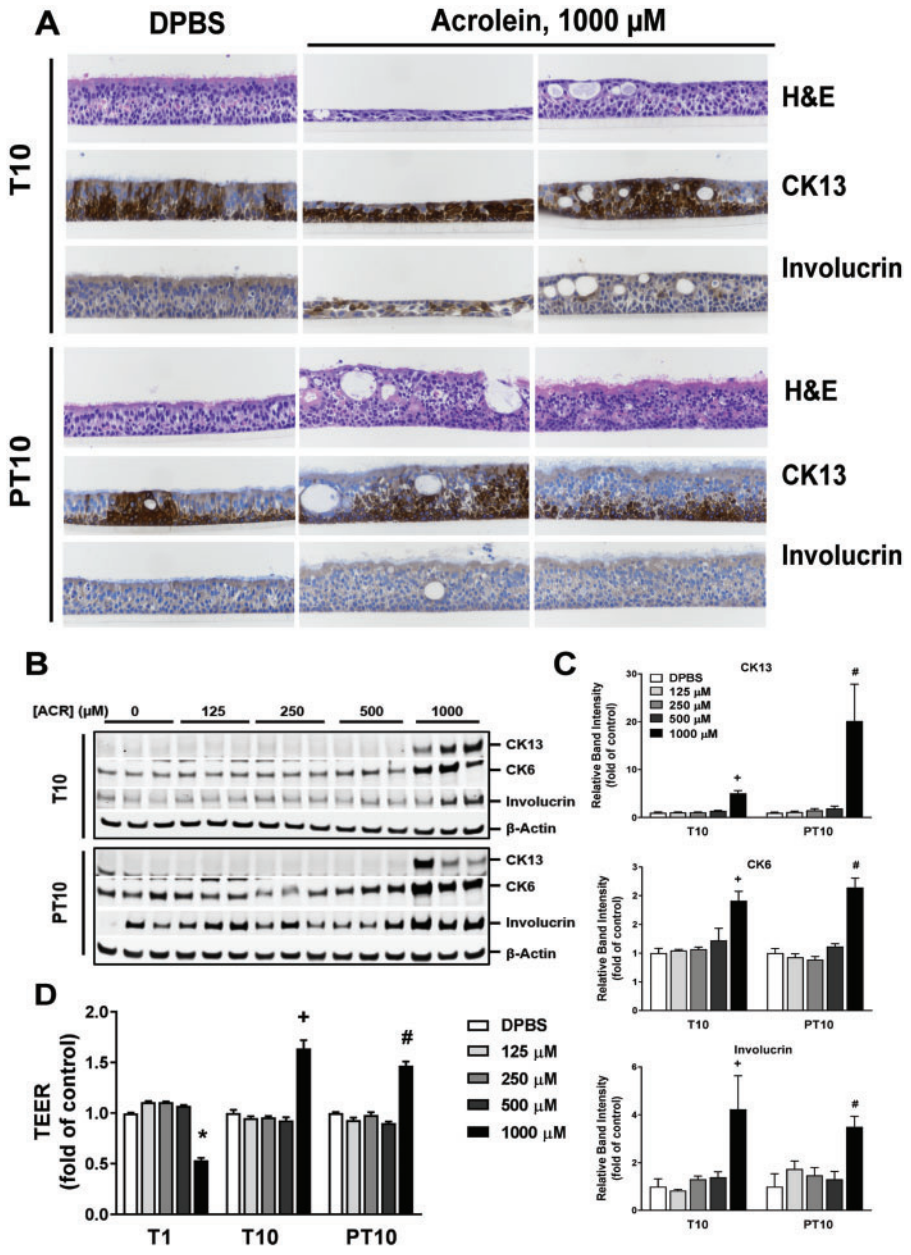

Figure 11. Induction of SQM differentiation and transformation by acrolein exposures. H&E and select markers for SQM were stained 24 h after 10 treatments (T10) and 24 h after a 10-day recovery (PT10) (A). Pictures were taken using 40× magnification. Protein expressions of three major SQM markers were evaluated in total cell lysate by immunoblotting (B). Densitometry was conducted to quantify the intensity of these bands and protein expressions are expressed as relative fold change to their corresponding β-actin loading control (C). TEER was measured 24 h after 1 (T1) and 10 treatments (T10) as well as 24 h after a 10-day recovery (PT10) (D). Data are expressed as means ± SEM ($n = 3$ for immunoblotting and TEER measurement and $n = 4$ for H&E and immunohistochemical staining). *, +, #$p < .05$ was considered statistically significant compared with their respective DPBS-treated controls.

Repetitive treatments, however, resulted in a significant and persistent reduction in CBF and possible damage or loss of ciliated cells as indicated by the decrease in acetylated α-tubulin protein expression. We hypothesize that acrolein-mediated cilia dysfunction may result from its reactivity with proteins in ciliated cells, such as cilia dynein adenosine triphosphatase and dynein (Sisson *et al.*, 1991). These findings are consistent with a report on the loss of ciliated cells in mice chronically exposed to cigarette smoke (Simet *et al.*, 2010). Considering that acrolein is a major toxic constituent of cigarette smoke, our findings suggest a role for acrolein in cigarette smoke-induced cilia toxicity.

Acrolein causes moderate to severe squamous hyperplasia and metaplasia over the entire respiratory tract in animal models (ATSDR, 2007; Beauchamp *et al.*, 1985). In the present study, we found that acrolein induced squamous differentiation in the ALI cultures as well as up-regulated expression of the squamous differentiation markers, CK6, CK13, and involucrin. After a 10-day recovery, a partial reversal of squamous differentiation, accompanied by a concurrent increase in the thickness of the epithelium, was observed. The persistent up-regulation of CK13 in acrolein-treated cultures suggests its role in cell proliferation, which subsequently may have contributed to the

increase in epithelial thickness (Costea *et al.*, 2003). It may be pertinent to note that the intraepithelial cysts observed in the acrolein-treated cultures may contain cell debris and thus, may also play an important role in acrolein-induced toxicity and tissue modeling. Interestingly, changes in TEER were temporally correlated with morphological alterations of the ALI cultures. Twenty-four hours after the first treatment, the TEER was decreased, suggesting a disruption of intercellular tight junctions and possible tissue damage; repetitive exposures, however, increased the TEER, which may have reflected the formation of squamous cells in the ALI cultures.

Overproduction of the pro-inflammatory cytokines, such as IL-1β, IL-6, and TNF-α, have been found in smokers with tracheobronchial SQM (Barnes, 2009). We, therefore, further examined the effects of acrolein on six disease-related cytokines, IL-1β, IL-6, IL-8, TNF-α, GM-CSF, and IFN-γ. Unexpectedly, the secretion of these cytokines was greatest following a single exposure, whereas repeated exposure attenuated their release. The early onset of acrolein-induced cytokine secretion suggests that such tissue responses may be mediated via activation of the extracellular signal-regulated kinase (ERK) and p38 mitogen-activated protein kinases (MAPKs) pathway (Finkelstein *et al.*, 2001). In contrast, prolonged treatments with acrolein may have inhibited NF-κB signaling and, therefore, abrogated cytokine expression (Li *et al.*, 1999). Given its continuous release induced by acrolein, IL-8 may have contributed to the squamous differentiation in the ALI cultures. It is noteworthy that addition of other cell types, such as fibroblast cells or macrophages, may influence pro-inflammatory responses in the ALI cultures. Such in vitro co-culture models, however, need to be extensively characterized for toxicity evaluation.

In addition to cytokines, MMPs also are involved in airway remodeling (Puchelle *et al.*, 2006). Several MMPs, predominantly MMP-1, -2, -8, -9, -12, and -14, can be activated by cigarette smoke and are associated with the development and exacerbation of COPD as well as emphysema (Barnes, 2004; Moretto *et al.*, 2012). Intriguingly, we found that acrolein modulated the secretions of MMP-7, -10, -12 and -13 throughout the treatment and recovery periods, while only MMP-13 levels were persistently increased suggesting it may be directly correlated with the squamous differentiation observed in the ALI cultures. However, we cannot exclude the possibility that the other MMPs, MMP-7, -10 and -12 may also play important roles in acrolein-induced tissue remodeling.

In summary, our study used a well-differentiated ALI human airway epithelial tissue model to identify a panel of respiratory disease-related toxicity events of acrolein exposure and defined their temporal concentration-response relationships. These findings demonstrate that repeated short exposure of the ALI cultures to acrolein induces tissue responses and histological alterations that are similar to those observed in animals and smokers with COPD (Bozinovski *et al.*, 2015; Churg *et al.*, 2008; Kirkham and Barnes, 2013). Our study not only reproduced the key toxicity events delineated in the MOA of acrolein toxicity, but also provides a better understanding of the strengths and limitations of applying advanced human in vitro tissue models for evaluating the toxicity of cigarette smoke and its constituents.

FUNDING

This work is supported by the U.S. Food and Drug Administration Center for Tobacco Products.

REFERENCES

Almolki, A., Guenegou, A., Golda, S., Boyer, L., Benallaoua, M., Amara, N., Bachoual, R., Martin, C., Rannou, F., Lanone, S., *et al.* (2008). Heme oxygenase-1 prevents airway mucus hypersecretion induced by cigarette smoke in rodents and humans. *Am. J. Pathol.* **173**, 981–992.

Andersen, M. E., and Krewski, D. (2010). The vision of toxicity testing in the 21st century: Moving from discussion to action. *Toxicol. Sci.* **117**, 17–24.

Araya, J., Cambier, S., Markovics, J.A., Wolters, P., Jablons, D., Hill, A., Finkbeiner, W., Jones, K., Broaddus, V.C., Sheppard, D., Barzcak, A., Xiao, Y., Erle, D.J., and Nishimur S.L. (2007). Squamous metaplasia amplifies pathologic epithelial-mesenchymal interactions in COPD patients. *J. Clin. Invest.* **117**, 3551–3562.

Agency for Toxic Substances and Disease Registry (ATSDR), US Public Health Service, Atlanta, GA. (2007). Toxicological Profile for Acrolein. http://www.atsdr.cdc.gov/toxprofiles/index.asp

Aufderheide, M., Scheffler, S., Ito, S., Ishikawa, S., and Emura, M. (2015). Ciliatoxicity in human primary bronchiolar epithelial cells after repeated exposure at the air–liquid interface with native mainstream smoke of K3R4F cigarettes with and without charcoal filter. *Exp. Toxicol. Pathol.* **67**, 407–411.

Augustyniak, E., Adam, A., Wojdyla, K., Rogowska-Wrzesinska, A., Willetts, R., Korkmaz, A., Atalay, M., Weber, D., Grune, T., Borsa, C., *et al.* (2015). Validation of protein carbonyl measurement: A multi-centre study. *Redox. Biol.* **4**, 149–157.

Avezov, K., Reznick, A. Z., and Aizenbud, D. (2014). Oxidative damage in keratinocytes exposed to cigarette smoke and aldehydes. *Toxicol. In Vitro* **28**, 485–491.

Barnes, P. J. (2004). Mediators of chronic obstructive pulmonary disease. *Pharmacol. Rev.* **56**, 515–548.

Barnes, P. J. (2009). The cytokine network in chronic obstructive pulmonary disease. *Am. J. Respir. Cell Mol. Biol.* **41**, 631–638.

Beauchamp, R. O., Andjelkovich, D. A., Kligerman, A. D., Morgan, K. T., and Heck, H. D. (1985). A critical review of the literature on acrolein toxicity. *CRC Crit. Rev. Toxicol.* **14**, 309–380.

Borchers, M.T., Wert, S.E., and Leikauf, G.D. (1998). Acrolein-induced MUC5ac expression in rat airways. *Am J Physiol.* **274**, L573–581.

Bozinovski, S., Vlahos, R., Anthony, D., McQualter, J., Anderson, G., Irving, L., and Steinfort, D. (2015). COPD and squamous cell lung cancer: Aberrant inflammation and immunity is the common link. *Br. J. Pharmacol.* **173**, 1–14.

Brunnemann, K. D., Kagan, M. R., Cox, J. E., and Hoffmann, D. (1990). Analysis of 1, 3-butadiene and other selected gas-phase components in cigarette mainstream and sidestream smoke by gas chromatography-mass selective detection. *Carcinogenesis* **11**, 1863–1868.

Burcham, P. C. (2004). Protein adduct-trapping by hydrazinophthalazine drugs: Mechanisms of cytoprotection against acrolein-mediated toxicity. *Mol. Pharmacol.* **65**, 655–610.

Burcham, P. C. (2017). Acrolein and human disease: Untangling the knotty exposure scenarios accompanying several diverse disorders. *Chem. Res. Toxicol.* **30**, 145–161.

Burcham, P. C., Raso, A., Thompson, C., and Tan, D. (2007). Intermolecular protein cross-linking during acrolein toxicity: Efficacy of carbonyl scavengers as inhibitors of heat shock potein-90 cross-linking in A549 cells. *Chem. Res. Toxicol.* **20**, 1629–1637.

Cai, J., Bhatnagar, A., and Pierce, W. M. (2009). Protein modification by acrolein: Formation and stability of cysteine adducts. *Chem. Res. Toxicol.* **22**, 708–716.

Cao, X., Lin, H., Muskhelishvili, L., Latendresse, J., Richter, P., and Heflich, R. H. (2015). Tight junction disruption by cadmium in an in vitro human airway tissue model. *Respir. Res.* **16**, 30.

Cao, X., Muskhelishvili, L., Latendresse, J., Richter, P., and Heflich, R. H. (2017). Evaluating the toxicity of cigarette whole smoke solutions in an air-liquid-interface human in vitro airway tissue model. *Toxicol. Sci.* **156**, 14–24.

Catilina, P., Thieblot, L., and Champelix, J. (1966). Experimental respiratory lesions by inhalation of acrolein in the rat. *Arch. Mal. Prof.* **27**, 857–867 (in French).

Choi, A. M., and Alam, J. (1996). Heme oxygenase-1: function, regulation, and implication of a novel stress-inducible protein in oxidant-induced lung injury. *Am. J. Respir. Cell Mol. Biol.* **15**, 9–19.

Churg, A., Cosio, M., and Wright, J. L. (2008). Mechanisms of cigarette smoke-induced COPD: Insights from animal models. *Am. J. Physiol. Lung Cell Mol. Physiol.* **294**, L612–L631.

Clippinger, A. J., Allen, D., Behrsing, H., BéruBé, K. A., Bolger, M. B., Casey, W., DeLorme, M., Gaça, M., Gehen, S. C., Glover, K., *et al.* (2018). Pathway-based predictive approaches for non-animal assessment of acute inhalation toxicity. *Toxicol. In Vitro* **52**, 131–145.

Comer, D. M., Elborn, J. S., and Ennis, M. (2014). Inflammatory and cytotoxic effects of acrolein, nicotine, acetylaldehyde and cigarette smoke extract on human nasal epithelial cells. *BMC Pulm. Med.* **14**, 11.

Corley, R. A., Kabilan, S., Kuprat, A. P., Carson, J. P., Jacob, R. E., Minard, K. R., Teeguarden, J. G., Timchalk, C., Pipavath, S., Glenny, R., *et al.* (2015). Comparative risks of aldehyde constituents in cigarette smoke using transient computational fluid dynamics/physiologically based pharmacokinetic models of the rat and human respiratory tracts. *Toxicol. Sci.* **146**, 65–88.

Corley, R. A., Kabilan, S., Kuprat, A. P., Carson, J. P., Minard, K. R., Jacob, R. E., Timchalk, C., Glenny, R., Pipavath, S., Cox, T., *et al.* (2012). Comparative computational modeling of airflows and vapor dosimetry in the respiratory tracts of rat, monkey, and human. *Toxicol. Sci.* **128**, 500–516.

Costea, D. E., Loro, L. L., Dimba, E. A., Vintermyr, O. K., and Johannessen, A. C. (2003). Crucial effects of fibroblasts and keratinocyte growth factor on morphogenesis of reconstituted human oral epithelium. *J. Invest. Dermatol.* **121**, 1479–1486.

Counts, M. E., Morton, M. J., Laffoon, S. W., Cox, R. H., and Lipowicz, P. J. (2005). Smoke composition and predicting relationships for international commercial cigarettes smoked with three machine-smoking conditions. *Regul. Toxicol. Pharmacol.* **41**, 185–227.

Cuervo, A. M., Bergamini, E., Brunk, U. T., Dröge, W., Ffrench, M., and Terman, A. (2005). Autophagy and aging: The importance of maintaining "clean" cells. *Autophagy* **1**, 131–140.

Davies, K. J. (2001). Degradation of oxidized proteins by the 20S proteasome. *Biochimie* **83**, 301–310.

Deshmukh, H. S., Shaver, C., Case, L. M., Dietsch, M., Wesselkamper, S. C., Hardie, W. D., Korfhagen, T. R., Corradi, M., Nadel, J. A., Borchers, M. T., *et al.* (2008). Acrolein-activated matrix metalloproteinase 9 contributes to persistent mucin production. *Am. J. Respir. Cell Mol. Biol.* **38**, 446–454.

Dong, J.-Z., Glass, J. N., and Moldoveanu, S. C. (2000). A simple GC-MS technique for the analysis of vapor phase mainstream cigarette smoke. *J. Microcolumn Sep.* **12**, 142–152.

Dorman, D. C., Struve, M. F., Wong, B. A., Marshall, M. W., Gross, E. A., and Willson, G. A. (2008). Respiratory tract responses in male rats following subchronic acrolein inhalation. *Inhal. Toxicol.* **20**, 205–216.

Fahy, J. V., and Dickey, B. F. (2010). Airway mucus function and dysfunction. *N. Engl. J. Med.* **363**, 2233–2247.

Finkelstein, E. I., Nardini, M., and van der Vliet, A. (2001). Inhibition of neutrophil apoptosis by acrolein: A mechanism of tobacco-related lung disease? *Am. J. Physiol. Lung Cell Mol. Physiol.* **281**, L732–L739.

Fulcher, M. L., Gabriel, S., Burns, K. A., Yankaskas, J. R., and Randell, S. H. (2005). Well-differentiated human airway epithelial cell cultures. *Methods Mol. Med.* **107**, 1083–1206.

Gao, W., Li, L., Wang, Y., Zhang, S., Adcock, I. M., Barnes, P. J., Huang, M., and Yao, X. (2015). Bronchial epithelial cells: The key effector cells in the pathogenesis of chronic obstructive pulmonary disease? *Respirology* **20**, 722–729.

Grafström, R. C., Dypbukt, J. M., Willey, J. C., Sundqvist, K., Edman, C., Atzori, L., and Harris, C. C. (1988). Pathobiological effects of acrolein in cultured human bronchial epithelial cells. *Cancer Res.* **48**, 1717–1721.

Hartung, T., and Daston, G. (2009). Are in vitro tests suitable for regulatory use? *Toxicol. Sci.* **111**, 233–237.

Hauber, H.-P., Foley, S. C., and Hamid, Q. (2006). Mucin overproduction in chronic inflammatory lung disease. *Can. Respir. J.* **13**, 327–335.

Julien, E., Boobis, A. R., Olin, S. S., and The ILSI Research Foundation Thresh. (2009). The key events dose-response framework: A cross-disciplinary mode-of-action based approach to examining dose-response and thresholds. *Crit. Rev. Food Sci. Nutr.* **49**, 682–689.

Kehrer, J. P., and Biswal, S. S. (2000). The molecular effects of acrolein. *Toxicol. Sci.* **57**, 6–15.

Kirkham, P. A., and Barnes, P. J. (2013). Oxidative stress in COPD. *Chest* **144**, 266–273.

Knowles, M. R., and Boucher, R. C. (2002). Mucus clearance as a primary innate defense mechanism for mammalian airways. *J. Clin. Invest.* **109**, 571–577.

Lemaître, V., Dabo, A. J., and D'Armiento, J. (2011). Cigarette smoke components induce matrix metalloproteinase-1 in aortic endothelial cells through inhibition of mTOR signaling. *Toxicol. Sci.* **123**, 542–549.

Li, L., Hamilton, R. F., and Holian, A. (1999). Effect of acrolein on human alveolar macrophage NF-kappaB activity. *Am. J. Physiol.* **277**, L550–L557.

LoPachin, R. M., Gavin, T., Petersen, D. R., and Barber, D. S. (2009). Molecular mechanisms of 4-hydroxy-2-nonenal and acrolein toxicity: Nucleophilic targets and adduct formation. *Chem. Res. Toxicol.* **22**, 1499–1508.

Loughlin, A. F., Skiles, G. L., Alberts, D. W., and Schaefer, W. H. (2001). An ion exchange liquid chromatography/mass spectrometry method for the determination of reduced and oxidized glutathione and glutathione conjugates in hepatocytes. *J. Pharm. Biomed. Anal.* **26**, 131–142.

Lushchak, V. I. (2012). Glutathione homeostasis and functions: Potential targets for medical interventions. *J. Amino Acids* **2012**, 736837–736863.

Moghe, A., Ghare, S., Lamoreau, B., Mohammad, M., Barve, S., McClain, C., and Joshi-Barve, S. (2015). Molecular mechanisms of acrolein toxicity: Relevance to human disease. *Toxicol. Sci.* **143**, 242–255.

Moretto, N., Volpi, G., Pastore, F., and Facchinetti, F. (2012). Acrolein effects in pulmonary cells: Relevance to chronic

obstructive pulmonary disease. *Ann. N. Y. Acad. Sci.* **1259**, 39–46.

National Research Council (US) Committee on Passive Smoking (1986) *Environmental Tobacco Smoke: Measuring Exposures and Assessing Health Effects*. The National Academies Press, Washington, DC.

O'Toole, T. E., Zheng, Y. T., Hellmann, J., Conklin, D. J., Barski, O., and Bhatnagar, A. (2009). Acrolein activates matrix metalloproteinases by increasing reactive oxygen species in macrophages. *Toxicol. Appl. Pharmacol.* **236**, 194–201.

Puchelle, E., Zahm, J.-M., Tournier, J.-M., and Coraux, C. (2006). Airway epithelial repair, regeneration, and remodeling after injury in chronic obstructive pulmonary disease. *Proc. Am. Thorac. Soc.* **3**, 726–733.

Rahimi, P. (1999). Monocyte inflammation augments acrolein-induced Muc5ac expression in mouse lung. *Endocrinology* **136**, 1–9.

Rigden, H. M., Alias, A., Havelock, T., O'Donnell, R., Djukanovic, R., Davies, D. E., and Wilson, S. J. (2016). Squamous metaplasia is icreased in the bronchial epithelium of smokers with chronic obstructive pulmonary disease. *PLoS One* **11**, e0156009.

Simet, S. M., Sisson, J. H., Pavlik, J. A., Devasure, J. M., Boyer, C., Liu, X., Kawasaki, S., Sharp, J. G., Rennard, S. I., and Wyatt, T. A. (2010). Long-term cigarette smoke exposure in a mouse model of ciliated epithelial cell function. *Am. J. Respir. Cell Mol. Biol.* **43**, 635–640.

Sisson, J.H., Tuma, D.J., and Rennard, S.I. (1991). Acetaldehyde-mediated cilia dysfunction in bovine bronchial epithelial cells. *Am J Physiol.* **260**, L29–36.

Sisson, J. H., Stoner, J. A., Ammons, B. A., and Wyatt, T. A. (2003). All-digital image capture and whole-field analysis of ciliary beat frequency. *J. Microsc.* **211**, 103–109.

Sun, Y., Ito, S., Nishio, N., Tanaka, Y., Chen, N., and Isobe, K. (2014). Acrolein induced both pulmonary inflammation and the death of lung epithelial cells. *Toxicol. Lett.* **229**, 384–392.

Tilley, A. E., Walters, M. S., Shaykhiev, R., and Crystal, R. G. (2015). Cilia dysfunction in lung disease. *Annu. Rev. Physiol.* **77**, 379–406.

U.S. Environmental Protection Agency. (2003). Integrated Risk Information System (IRIS) Toxicological review of acrolein. https://cfpub.epa.gov/ncea/risk/recordisplay.cfm?deid=51977

U.S. Environmental Protection Agency, Risk assessment forum, Washington, DC. (2005). Guidelines for carcinogen risk assessment.

Walker, T. R., and Kiefer, J. E. (1966). Ciliastatic components in the gas phase of cigarette smoke. *Science* **153**, 1248–1250.

Yeager, R. P., Kushman, M., Chemerynski, S., Weil, R., Fu, X., White, M., Callahan-Lyon, P., and Rosenfeldt, H. (2016). Proposed mode of action for acrolein respiratory toxicity associated with inhaled tobacco smoke. *Toxicol. Sci.* **151**, 347–364.